Article

Journal of
Nanoscience and Nanotechnology
Vol. 19, 7974–7981, 2019
www.aspbs.com/jnn

Core–Shell Palladium Telluride Quantum Dot-Hemethiolate Cytochrome Based Biosensor for Detecting Indinavir Drug

Usisipho Feleni[1,2,*], Unathi Sidwaba[1,2], Hlamulo Makelane[1], and Emmanuel Iwuoha[1,*]

[1] *SensorLab, Department of Chemistry, University of Western Cape, P. Bag X17, Bellville, Cape Town, 7535, South Africa*
[2] *Nanotechnology and Water Sustainability Research Unit, College of Science, Engineering and Technology, University of South Africa, Florida Campus, Roodepoort, 1709, Johannesburg, South Africa*

Indinavir is a first-generation HIV protease inhibitor anti-retroviral (ARV) drug. Due to interindividual differences in the rate of indinavir metabolism, clinicians and pharmacologists have expressed urgent need for sensor devices that will enable real time determination of appropriate dosage. In this study, an indinavir biosensor was developed by the functionalization of a cysteamine-modified gold (Cyst|Au) electrode with biocompatible core–shell 3-mercaptopropionic acid (3-MPA)-capped palladium telluride quantum dot (PdTeQD) and the heme-thiolate cytochrome P450-3A4 (CYP3A4) enzyme. The PdTeQD was capped with 3-mercaptopropionic acid (3-MPA) to improve its reactivity, biocompatibility and thermal stability. Small angle X-ray scattering (SAXS) studies revealed that the 3-MPA-PdTeQD particles formed core–shells with diameters of 4.7 nm. Fourier transformed infrared spectroscopy (FTIR) experiments confirmed the formation of 3-MPA-PdTeQD by the presence of specific COOH and CH_2 FTIR signature bands. Ultraviolet-visible (UV-Vis) spectrophotometric analysis of the quantum dot, exhibited a broad characteristic band at ∼320 nm, corresponding to a band gap energy (E_g) value of 3.87 eV, indicating that the QD is a semiconducting material. Cyclic voltammetry (CV) responses of the biosensor (i.e., CYP3A4|3-MPA-PdTeQD|Cyst|Au) indicated that 0.26 V was the suitable potential for measuring indinavir metabolism. The biosensor has a sensitivity, dynamic linear range (DLR) and limit of detection (LOD) values of 0.0218 μA/nM, 0.0004–0.01 nM (i.e., $3\times10^{-7}-7\times10^{-6}$ mg L^{-1}) and 0.023×10^{-7} mg L^{-1}, respectively, for indinavir. The LOD value was lower than the maximum plasma concentration (C_{max}) value (0.13–8.6 mg L^{-1}) of indinavir which is normally measure 8 h after intake. The low DLR value makes the biosensor suitable for application at point-of-care, where indinavir concentration is expected to be in ng L^{-1} level in physiological samples within a few minutes of the drug administration.

Keywords: Anti-Retroviral Drug, Cytochrome P450-3A4 Enzyme, Drug Metabolism, Electrochemical Biosensors, Indinavir, Palladium Telluride Quantum Dot.

1. INTRODUCTION

The synthesis and application of high quality thiol-capped QD have generated great interest in various fields of biology; in-bio-labelling[1] and biosensing.[2] In comparison with traditional materials for the development of sensors such as fluorescent organic labels, carbon materials and graphene, QD are known to be superior in performance due to numerous advantages such as brightness, extraordinary photostability, broad excitation wavelength range, and size-tunable narrow, symmetric emission spectra ranging from 400 to 2000 nm and multicolor light emission.[3–5] The QD fascinating and outstanding optical features make them more suitable for biological labeling and have inspired scientists and provided an incredible platform for researchers to investigate their applications in different fields.[6,7] Aqueous solubility and functionalization of QD materials are regarded as the most common problem for application in biological studies.[8] Therefore, the introduction of stabilizing agents would play an important role in controlling the particle size and distribution

*Authors to whom correspondence should be addressed.

 1533-4880/2019/19/7974/008 doi:10.1166/jnn.2019.16866

and, hence, the catalytic activity of quantum dots. The surface functionalization of QD materials with amphiphilic bi-functional molecules such as mercapto carboxylic acids like 3-mercapotpropionic acid (3-MPA) which is reported in this paper leads into the formation of small sized nanomaterials which would promote the transfer of electrons during analysis.[9, 10] During the construction of the biosensor system, the issue of the biocompatibility should be considered because the biological recognition molecules such as enzymes may lose their activity at biologically incompatible environments.[11, 12]

Therefore, the combination of semiconductor QD materials and CYP450 enzymes bring more opportunities in electroanalysis such as the improvement of bioelectrode performance in terms of sensitivity and specificity.[13, 14] Thus, in this work we focused on the optical and electronic properties as well as the biocompatibility of high quality 3-MPA-PdTeQD, which was applied as an alternative functional bio-material to accelerate electron transfer in the development of electrochemical biosensor system. Herein, an electrochemical biosensor system was produced by incorporating 3-MPA-PdTeQD and cytochrome P450-3A4 (CYP3A4) enzyme on a self-assembled monolayer cysteamine (Cyst) modified gold electrode surface for the determination of protease inhibitor-indinavir drug administered for HIV/AIDS-related infections.

2. EXPERIMENTAL DETAILS

2.1. Chemicals and Solutions

All reagents were of analytical grade and used without any further purification. The reagents include palladium chloride ($PdCl_2$, 99.9%), tellurium powder (Te, 99.997%) 3-mercaptopropionic acid [$HSCH_2CH_2CO_2H$] (3-MPA, ≥99%), sodium hydroxide (NaOH, ≥99%), sodium borohydride ($NaBH_4$, 98%), hydrogen chloride (HCl, 37%) 1-ethyl-3-(3-dimethylaminopropyl) carbodiimide hydrochloride (EDC, 98%), N-hydroxysuccinimide (NHS, 98%), sodium phosphate monobasic dehydrate ($H_2NaPO_4 \cdot 2H_2O$, >99%), disodium hydrogen phosphate dibasic ($Na_2PO_4 \cdot 2H_2O$, >98%), cysteamine (C_2H_7NS, ≥98%; Cyst) and human cytochrome P450-3A4 enzyme (≥50 units/mg protein based on reductase activity) expressed in *Saccharomyces cerevisiae* were all purchased from Sigma Aldrich, and stored in the freezer at −70 °C when not in use. Electrolyte solution of 0.1 M phosphate buffer solution, pH 7.4 was prepared by mixing stock standard solution of 0.1 M disodium hydrogen phosphate dibasic and sodium dihydrogen phosphate monobasic using Milli Q water purification and was used as a supporting electrolyte in all the experiments. All experiments were conducted at room temperature (23 °C) unless otherwise stated. Stock and working standard solutions of indinavir were freshly prepared from Indinavir sulphate, obtained through extraction from the capsules Crixivan 400 mg (M.W. 711.88) and purchased from Merck & Co., Inc., NJ, USA, in 0.1 M PBS, pH 7.4. The prepared solutions were kept at 4 °C until used. Alumina micro polish and polishing pads were obtained from Buehler, IL, USA and were used for cleaning the gold electrode prior any modification. For the preparation of water-soluble and biocompatible PdTeQD, all glassware used was cleaned in a freshly prepared strong acid solution of 3:1 HCl/HNO_3 followed by thoroughly rinsing the glassware with deionized water to ensure that it was properly cleaned.

2.2. Instrumentation

Electrochemical responses of the biosensor system were investigated by cyclic voltammetry under aerobic conditions. The voltammograms were acquired using a 273A Potentiostat/Galvinostat (Princeton Applied Research), wherein gold electrode (3 mm in diameter), platinum wire and Ag/AgCl (3 M NaCl type) acted as the working electrode, the counter electrode and the reference electrode, respectively. Cyclic voltammetry (CV) experiments were performed in 0.1 M PBS over a potential range of +1.5 V to −1.5 V to cover all reactions of interest in the investigated system. The employed potential range was scanned in both positive and negative sweeps with various scan rates (5–50 mV/s) for the sensor platform and (50–500 mV/s) for electrochemical biosensor responses to indinavir. For detailed analysis, CV scans were registered at a scan rate of 500 mV/s. Ultraviolet-visible (UV-Vis) absorption measurements for the prepared 3-MPA-PdTeQD were obtained using 1 cm quartz cuvette on a Nicolet Evolution 100 UV-visible spectrophotometer (Thermo Electron, UK) over a wavelength range of 200 to 800 nm. Fluorescence emission spectra were measured using a Nanolog spectrofluorometer (Horiba Jobin Yvon, USA) with a slit width of 5 nm. Fourier transformed infrared (FTIR) spectra were recorded on a Perkin Elmer FTIR model 100 spectrometer in the region of 400 to 4000 cm^{-1} wavenumber range to determine the characteristic features of 3-MPA-PdTeQD. The morphology, size and shape, composition, and microstructures of the obtained QD were characterized by scanning electron microscopy (SEM, Zeiss Auriga S40) operating at 50 kV, high-resolution transmission electron microscopy (HRTEM, FEI Tecnai G220) equipped with an energy-dispersive spectroscopy (EDS) detector. A drop of 3-MPA-PdTeQD material was deposited on a 300 mesh formvar-carbon coated grid and dried at room temperature. Small-Angle X-ray Scattering (SAXS) (Anton Paar, GmbH, Australia) measurements were obtained using a 1 mm diameter quartz capillary positioned at a distance of 317 mm from the SDD camera and temperature-controlled at 20 °C. For each measurement, six frames were obtained at 100 s exposure time and averaged. The deionized water which acted as a reference was measured under the same conditions as the QD material. Data evaluation/analysis was performed with the GIFT software (generalized indirect Fourier transformation (GIFT)).

2.3. Synthesis of Water-Soluble 3-MPA-PdTeQD

The experimental procedure was performed in accordance with previous studies,[15] with some modifications. First, palladium precursor was prepared in a three necked-round bottomed flask by dissolving $PdCl_2$ (0.332 g, 1.875 mmol) and 3-MPA (490 μL, 5.625 mmol) in 10 mL of deionized water, under nitrogen atmosphere and constant stirring. The pH of the solution was adjusted to 11.4 by adding 1 M sodium hydroxide (NaOH). In a second reaction flask, NaHTe solution was prepared by mixing tellurium powder (Te) (0.319 g, 1.25 mmol) and sodium borohydride ($NaBH_4$) (0.189 g, 2.5 mmol) in 10 mL deionized water and covered with aluminum foil at room temperature for 30 min until the solution attained a light purple color. Then, 5 mL of NaHTe solution was injected into the nitrogen saturated palladium precursor flask and a colour change was observed from reddish to dark orange indicating the initiation of nucleation of the QD. The resulting solution was stirred and heated up to (100 °C) and aliquots of the reaction solution were removed at regular intervals for the UV-Vis and PL analyses.

2.4. Preparation of CYP3A4 Biosensor System

The indinavir electrochemical biosensor system was prepared by first polishing the AuE with 1, 0.3 and 0.05 μm alumina slurries and thoroughly rinsed with deionized water after each polishing step. After that, the cleaned Au electrode surface was dipped in 200 μL of 0.02 M cysteamine aqueous solution and kept in the dark for 24 h to form a monolayer through Au–S covalent bonding. Then, the Cyst/Au modified electrode was carefully rinsed with water to remove any physically adsorbed Cyst. For the covalent coupling of highly monodispersed 3-MPA-PdTeQD, a 3 μL drop of a solution consisting of 3-MPA-PdTeQD was mixed together with 1 μL of 1-ethyl-3-[3-dimethylaminopropyl]carbodiimide/N-hydroxysuccinimide (EDC/NHS, ratio 1:1) and placed onto Cyst/Au modified electrode for 12 h. The film of material on the electrode surface was rinsed with 0.1 M PBS, to remove unbound PdTeQD material. Lastly, an aliquot of 3 μL CYP450-3A4 thiolate enzyme solution was then drop-casted onto 3-MPA-PdTeQD|Cyst|Au modified electrode surface and allowed to dry for 3 h, at 4 °C. The resulting CYP3A4|3-MPA-PdTeQD|Cyst|Au was stored at 4 °C in 0.1 M PBS when not in use. For comparison, bare Au, 3-MPA-PdTeQD and CYP3A4|Au modified electrodes were also prepared.

3. RESULTS AND DISCUSSION

3.1. Crystal Structure of 3-MPA-PdTeQD

Stabilizing agents play an outstanding role in particle size reduction and distribution of quantum dots.[16] Interestingly, a capping agent that binds strongly with quantum dots surface can effectively stabilize and form smaller sizes of as-prepared quantum dots.[17–19] In this study, small angle X-ray scattering (SAXS), high-resolution transmission and scanning electron microscopy techniques (TEM, SEM) were mainly aimed to determine the precise size distribution, shape, electron density contrast as well as the chemical composition of the synthesized QD material.[20] As can be seen in Figure 1(a) the free model pair-distance distribution function (PDDF) of 3-MPA-PdTeQD possess a characteristic profile, typically observed for core–shell particles with identical sizes (maximum diameter size of 4.7 nm). In addition, the size distribution by number (shown in the insert of Fig. 1(a)) was calculated with program GIFT where the 3-MPA-PdTeQD revealed highly monodispersed particles with an average radius of approximately 2 nm.[20] The 3-MPA-PdTeQD micrographs observed in Figure 1(b) and its insert revealed non-agglomerated, uniformly distributed spherical structures with well-resolved lattice fringes[21–23] and are in diameter range of 2 nm.[24] The well resolved lattice fringes confirmed the good crystallinity of 3-MPA-PdTeQD.[25,26] Moreover, non-agglomeration of nanoparticles resulted from electrostatic repulsion of negatively charged dehydrogenated carboxylic groups present in 3-MPA capping agent.[27,28] In contrast with SAXS and HRTEM, HRSEM (Fig. 1(c)) of the 3-MPA-PdTeQD exhibited agglomerated spherical bubbles with collection of different sizes approximately 200 nm.[29] The observed agglomeration was attributed to a small volume of stabilizing agent used during the synthesis which caused an increase in the surface area to volume ratio and hence increased the attractive forces between the nanoparticles thereby causing them to agglomerate.[30] This observation was further confirmed by energy-dispersive X-ray spectroscopy EDX in (Fig. 1(d)), which revealed the presence of Pd, Te and S in PdTeQD sample which are the main components of the as-prepared material. The obtained results are similar to the previous reports performed in our lab by various authors using different QDs capped with 3-mercaptopropionic acid. For instance, Ndangili and coworkers[2] reported 3-MPA-ZnSeQD which revealed crystallinity and monodispersed QDs with average size 4 nm in diameter.

3.2. Optical Properties of 3-MPA-PdTeQD

Palladium telluride quantum dots (PdTeQD) have unique optical, electrical and thermal properties and are being incorporated into various electrochemical biosensors.[25,31] The UV-vis and PL analysis were carried out to investigate the absorption, emission and excitation wavelength of 3-MPA-PdTeQD. The UV-vis spectrum showing remarkable optical properties of PdTeQD is illustrated in Figure 2(a). Three absorbance bands are observed at 240 nm, 275 nm and 320 nm, respectively. The first absorbance band appearing at higher energy (240 nm) was attributed to the metal-to-ligand charge transfer (i.e., palladium ions and thioglycolic acid capping agent) while the absorbance band at 275 nm was ascribed to $n \rightarrow \sigma^*$ transitions of thiol groups on the 3-MPA.[32] Notably, PdTeQD

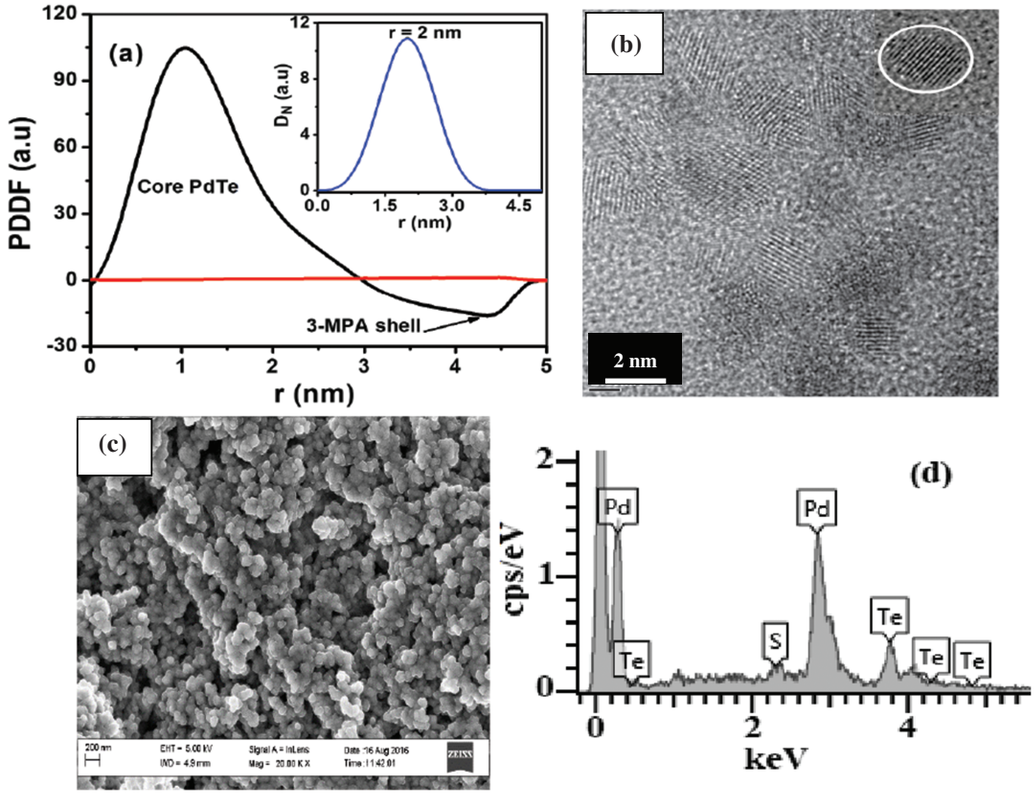

Figure 1. (a) SAXS pair-distance distribution function (PDDF). (Insert: SAXS size distribution by number). (b) HR-TEM micrograph of 3-MPA-PdTeQD at 2 nm scale view. (c) HR-SEM micrograph of 3-MPA-PdTeQD. (d) EDX spectrum revealing elemental composition of a selected region.

exhibited a broad absorbance band at 320 corresponding to the band gap energy (E_g) value of 3.87 eV (which is within the range of E_g values for QD particles), that confirmed the successful synthesis of the QDs. Due to the broad absorbance band of PdTeQD, the band gap difference between different sizes of the QD would be wider and hence result in an improvement of the confinement of electrons and holes.[33] However, the absorption band around 410 nm due to the absorption of Pd(II) ions was not observed (Fig. 2(a)), which is an evidence that the Pd(II) ions that were present in $PdCl_2$ were properly reduced to Pd^0.[34] The normalized PL spectra for the five aliquots taken during synthesis are shown in Figure 2(b). The residual blue shift in emission bands seen around 510–460 nm associated with band gap energies (2.4 eV–2.7 eV) were attributed to the surface defects upon passivation of 3-MPA and PdTeQD.[35] Additionally, this blue shift of fluorescence emission bands over refluxing period provided an evidence for the occurrence of the band-gap broadening phenomenon due to the quantum size effect which confirmed the successful coating of the PdTe core. Furthermore, the broad emission peaks observed indicated that the 3-MPA-PdTeQD have broad dispersity which is in accordance with the information obtained from the absorption spectra of these QD.

3.3. Structural Properties of 3-MPA-PdTeQD

FTIR spectroscopy was employed to investigate the characteristic features of 3-mercaptopropionic acid capping agent adsorbed onto the surface of synthesized PdTeQD. It was expected that the thiol group (–SH) of the 3-MPA which is hydrophilic would covalently bind with the hydrophobic surface of the quantum dot while the carboxylic acid group (–COOH) extends water molecule to make the quantum dot soluble and can be conjugated with bioagents, enabling their application in biosensor fabrication.[26] Figure 3 represents the FT-IR spectra of (a) 3-MPA (black line) and (b) 3-MPA-PdTeQD (red line). The spectrum of 3-MPA exhibited five absorption bands at ~2950 cm^{-1}, 2550 cm^{-1}, 1660 cm^{-1}, 1402 cm^{-1} and 1213 cm^{-1} which were attributed to an O–H stretch (which confirmed the good dispersion of the quantum dot in water and other biological media), S–H stretch, C═O stretch, which represents the carboxyl group and existence asymmetric stretching of C–H.[36, 37] In contrast, the spectrum of the capped PdTeQD sample displayed absorption bands assigned to the carboxylate anion of the surface ligands. The carboxylate anion on the QD was formed during the synthesis process, in which the NaOH used to adjust the pH to 11.4 deprotonated the COOH group. However, the shift in wavenumbers and the decrease in C═O

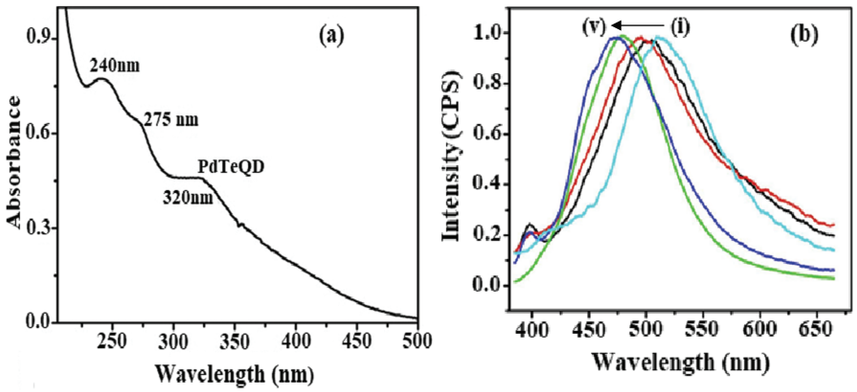

Figure 2. (a) UV-Vis spectrum of 3-MPA-PdTeQD obtained in 0.1 M PBS (pH 7.4). (b) Normalized PL spectra of 3-MPA-PdTeQD recorded at (i) 20 min, (ii) 30 min, (iii) 40 min, (iv) 50 min, and (v) 60 min.

stretch, as well as, the disappearance of the S–H stretch confirmed the formation of S–PdTe bonds between MPA and the PdTe core,[38] as illustrated in Figure 3(b).

3.4. Electrochemistry of 3-MPA-PdTeQD

3.4.1. Voltammetric Studies of 3-MPA-PdTeQD

The electrocatalytic properties of 3-MPA-PdTeQD modified electrode and bare Au electrode were studied by cyclic voltammetry (CV). For the bare electrode (Fig. 4(i)), the voltammetric response revealed one cathodic peak ($E_{pc} = 0.46$ V) and interestingly, one anodic peak ($E_{pc} =$ 0.83 V), which reflected the reduction and subsequent oxidation of the gold oxide.[39] When 3-MPA-PdTeQD were deposited on a gold electrode surface, a distinctive number of cathodic peaks were observe at $E_{pc} = 0.12$ V (peak A_1), −0.05 V (peak A_2), −0.252 V (peak A_3), −0.75 V (peak A_4) and −1.1 V (peak A_5) (Fig. 4(ii)), while three distinct anodic peaks appeared at {1.2 V (peak C_1), 0.45 V (peak C_2) and −0.33 V (peak C_3)}, respectively. For peak (A_1), the observed cathodic peak was attributed to Te^{4+} ions generated from QD oxidation. Additionally, the observed cathodic peak (A_2) corresponded to the reduction of Te^{4+} to Te^0 while the cathodic peak (A_3) was responsible for further reduction of Te^0 to Te^{2-}.[40] As inspected carefully, peak (A_2) appeared at higher current than (A_3) thus indicating that both A_2 and A_3 are associated with the reduction of metallic oxidation of the QD. Moreover, a characteristic cathodic peak (A_4) observed at −0.75 V was most likely associated with the reduction of the PdTeQD. The anodic peaks observed at (C_1) and (C_2) were attributed to Pd^{2+} ions generated from the oxidation of PdTeQD and the interaction between the metal-to-ligand charge transfer i.e., (Pd-3-MPA).[41] In addition to this, the observed anodic peak (C_3) corresponded to the oxidation of PdTeQD.

3.4.2. Biosensor Responses to Indinavir Drug

Direct electrochemistry of CYP3A4 enzyme was employed in this work to create a desirable model for fundamental study of the redox behavior of the proteins in biological systems. This would give a full detailed explanation about the mechanisms of redox transformations of

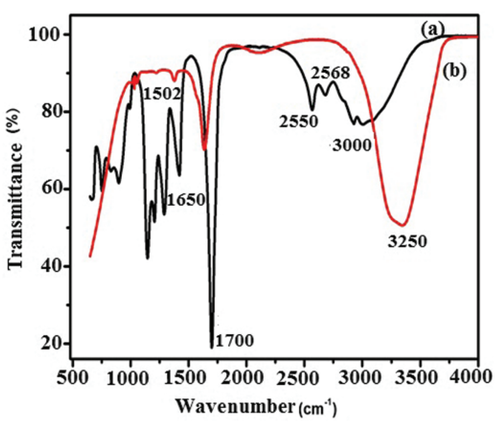

Figure 3. FT-IR spectra of (a) 3-MPA capping agent and (b) 3-MPA-PdTe QD.

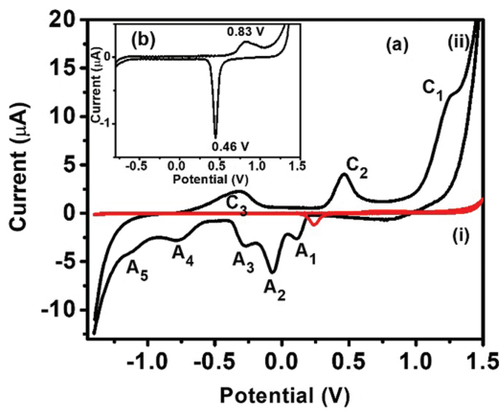

Figure 4. (a) Cyclic voltammograms of (i) bare Au and (ii) 3-MPA-PdTeQD|Au electrodes recorded in 0.1 M PBS (pH 7.4) at 21 mV/s. (b) A magnified voltammogram of the bare Au electrode.

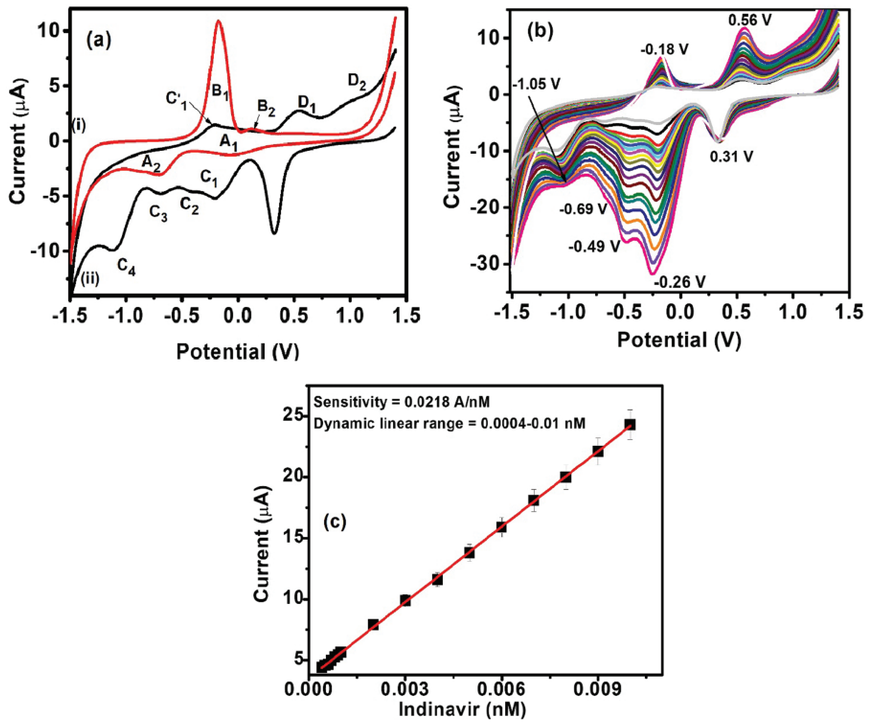

Figure 5. (a) Cyclic voltammograms of (i) CYP3A4|Au and (ii) CYP3A4|3-MPA-PdTeQD|Cyst|Au electroenzyme biosensors. (b) Electrochemical responses of CYP3A4|3-MPA-PdTeQD|Cyst|Au electroenzyme biosensor to indinavir. (c) The calibration plot of the CYP3A4|3-MPA-PdTeQD|Cyst|Au electroenzyme biosensor.

protein molecules as well as their metabolic processes involving redox transformations.[42] The CV shown in Figure 5(a(i)) demonstrates the electrochemical behavior of CYP3A4 enzyme immobilized on the bare Au electrode. Two cathodic peaks were observed at −0.05 V (peak A_1) and −0.69 V (peak A_2), with two anodic peak which appeared at −0.18 V (peak B_1) and 0.12 V (peak B_2). The observed cathodic peak at −0.05 V was attributed to the reduction of the heme group from CYP3A4 (Fe^{III}) to CYP3A4 (Fe^{II}) in the presence of oxygen,[43] while the reduction peak at −0.69 V was ascribed to the monooxgyenation process. Moreover, the oxidation peak at −0.18 V appeared at a very high current intensity due to the re-oxidation of CYP3A4 (Fe^{II}) to CYP3A4 (Fe^{III}). This peak would increase or decrease in the presence of a substrate/inhibitor of the enzyme.[44] The estimated potential value for the immobilized CYP3A4 enzyme is not the same as other researchers reported.[45] This may be attributed to the possible differences in the heme center of P450 in solution and its immobilized state.

In comparison with CYP3A4|Au, CYP3A4|3-MPA-PdTe|Cyst|Au biosensor system illustrated in Figure 5(a(ii)) exhibited four cathodic peaks at −0.21 V (peak C_1), −0.44 V (peak C_2), −0.7 V (peak C_3) and −1.1 V (peak C_4) with three anodic peaks at −0.21 V (peak C'_1), 0.5 V (peak D_1) and 0.97 V (peak D_2), respectively. The observed reduction peaks were attributed to the redox of the electroactive heme center of the immobilized protein coupling between $–NH_2$ and –COOH of 3-MPA-PdTeQD which acted as a mediator by shuttling electrons to and from the enzyme to speed up the reaction.[46] Such results strongly suggested that 3-MPA-PdTeQD play an important role in improving the bioactivity of CYP3A4 and in promoting electron transfer between CYP3A4 and the electrode.[43, 45]

Figure 5(b) illustrates the CV responses of the biosensor under aerobic conditions, in the presence and absence of indinavir in 0.1 PBS, pH 7.4 scanned from −1.5 V to 1.5 V at 500 mV/s. The aerobic conditions in the reaction was necessary for the monooxgyenation reaction (i.e., the binding of molecular oxygen (O_2) to CYP3A4 (Fe^{2+}) to form Fe–O center in order to observe enzyme-oxygen substrate interactions.[47] In the absence of indinavir drug, the biosensor system consisted of reduction and oxidation waves, with cathodic peaks and anodic peaks, at potential values of (−0.26 V, −0.49 V, −0.69 V and −1.05 V) and (−0.18 V and 0.56 V), respectively. Upon the addition of different concentrations of indinavir, a remarkable enhancement in the cathodic peak currents with slight shifts were obtained in the presence of oxygen binding to the active site of the heme center of the enzyme.[48] This characteristic process has been documented in literature reports about biosensor studies with P450.[49] In contrast with other reduction peaks, the major cathodic peak considered for indinavir responses was observed at −0.26 V. It is known that the binding of substrates to the

ferric CYP (Fe^{III}) changes the spin state from low spin to high spin and makes the redox potential of the enzyme shift towards more positive potentials, thus promoting the electron transfer to and from the electrode system.[50, 51] In addition, the CYP3A4-indinavir binding at −0.26 V boosted the reduction of CYP to its ferrous form, resulting in a faster oxygen binding. Therefore, the observed characterisitc features of the modified electrode offer enormous promise for its sensing applications.

The linear calibration of the indinavir biosensor (CYP3A4|3-MPA-PdTeQD|Cyst|Au) is shown in Figure 5(c); which is actually a plot of the dynamic linear range (DLR) of 0.0004 to 0.01 nM (i.e., 3×10^{-7}–7×10^{-6} mg L^{-1}) of the biosensor. A sensitivity value of 0.0218 μA/nM and a limit of detection limit (LOD) value of 0.023×10^{-7} mg L^{-1} were obtained. Ross and co-workers[49] reported an LOD value of 7.1×10^{-4} mg L^{-1} for indinavir. The comparatively low LOD value obtained for CYP3A4/3-MPA-PdTeQD/Cyst/Au biosensor in this study, implies that it will be very suitable for measuring the low concentrations of indinavir (expected for testing metabolic rate at point-of-care) and can be also be customized for higher concentrations.

4. CONCLUSION

A highly sensitive electrochemical indinavir biosensor (CYP3A4|3-MPA-PdTeQD|Cyst|Au), which had a low operational potential of −0.26 V, was successfully developed. SAXS, HR-TEM and HR-SEM studies revealed that the 3-MPA-PdTeQD used as sensor platform consisted of spherical core shell units with a maximum size of 4.7 nm. The biosensor performance indecies include: sensitivity (0.0218 μA/nM), DLR (0.0004–0.01 nM, i.e., 3×10^{-7}–7×10^{-6} mg L^{-1}) and LOD (0.023×10^{-7} mg L^{-1}). The indinavir maximum plasma concentration (C_{max}) value (0.13–8.6 mg L^{-1}), is much higher than both the DLR and LOD values of the indinavir biosensor (CYP3A4|3-MPA-PdTeQD|Cyst|Au). Thus, the biosensor is suitable for the detection of extremely low levels of indinavir expected in physiological samples, when orally administered to patient within the short consultation period at point-of-care.

Acknowledgments: This work was partially funded by the South African Department of Science and Technology's (DST's) National Nanoscience Postgraduate Teaching and Training Platform (NNPTTP).

References and Notes

1. Walling, M.A., Novak, J.A. and Sheperd, J.R.E., **2009**. Quantum dots for live cell and *in vivo* imaging. *International Journal of Molecular Sciences, 10*(2), pp.441–491.
2. Ndangili, P.M., Arotiba, O.A., Baker, P.G.L. and Iwuoha, E.I., **2010**. A potential masking approach in the detection of dopamine on 3-mercaptopropionic acid capped ZnSe quantum dots modified gold electrode in the presence of interferences. *Journal of Electroanalytical Chemistry, 643*(1–2), pp.77–81.
3. Sun, H., Wu, L., Wei, W. and Qu, X., **2013**. Recent advances in graphene quantum dots for sensing. *Materials Today, 16*(11), pp.433–442.
4. Lim, S.J., Zahid, M.U., Le, P., Ma, L., Entenberg, D., Harney, A.S., Condeelis, J. and Smith, A.M., **2015**. Brightness-equalized quantum dots. *Nature Communications, 6*, pp.1–10.
5. Medintz, I.L., Uyeda, H.T., Golman, E.R. and Mattoussi, H., **2005**. Quantum dot bioconjugates for imaging, labelling and sensing. *Nature Materials, 4*(6), pp.435–446.
6. Yue, Z., Lisdat, F., Parak, W.J., Hickey, S.G., Tu, L., Sabir, N., Dorfs, D. and Bigall, N.C., **2013**. Quantum-dot-based photoelectrochemical sensors for chemical and biological detection. *ACS Applied Materials and Interfaces, 5*(8), pp.2800–2814.
7. Arivarasan, A., Bharathi, S., Vijayaraj, V., Sasikala, G. and Jayavel, R., **2018**. Evaluation of reaction parameters dependent optical properties and its photovoltaics performances of CdTe QDs. *Journal of Inorganic Organometallic Polymers and Materials*, *28*(3), pp.1263–1275.
8. Jin, S., Hu, Y., Gu, Z., Liu, L. and Wu, H.-C., **2011**. Application of quantum dots in biological imaging. *Journal of Nanomaterials, 2011*, pp.1–13.
9. Feleni, U., Ajayi, R.F., Jijana, A., Sidwaba, S., Douman, F., Baker, G.G.L. and Iwuoha, E., **2016**. Tin selenide quantum dots electrochemical biotransducer for the determination of indinavir—A protease inhibitor anti-retroviral drug. *Journal of Nano Research, 44*, pp.196–207.
10. Petkova, G.A., Záruba, K., Žvátora, P. and Král, V., **2012**. Gold and silver nanoparticles for biomolecule immobilization and enzymatic catalysis. *Nanoscale Research Letters, 7*, pp.1–10.
11. Singh, E., Meyyappan, M. and Nalwa H.S., **2017**. Flexible graphene-based wearable gas and chemical sensors. *ACS Applied Materials and Interfaces, 9*(40), pp.34544–34586.
12. Grieshaber, D., MacKenzie, R., Vörös, J. and Reimhult, E., **2008**. Electrochemical biosensors—sensor principles and architectures. *Sensors, 8*(3), pp.1400–1458.
13. Zhu, C., Yang, G., Li, H., Du, D. and Lin, Y., **2015**. Electrochemical sensors and biosensors based on nanomaterials and nanostructures. *Analytical Chemistry, 87*(1), pp.230–249.
14. Singh, R., Singh, E. and Nalwa, H.S., **2017**. Inkjet printed nanomaterial based flexible radio frequency identification (RFID) tag sensors for the internet of nano things. *RSC Advances, 7*(77), pp.48597–48630.
15. Mazing, D.S., Brovko, A.M., Matyushkin, L.B., Aleksandrova, O.A. and Moshnikov, V.A., **2015**. Preparation of cadmium selenide colloidal quantum dots in non-coordinating solvent octadecene. *Journal of Physics: Conference Series, 661*, Article ID 012033, 4 pages.
16. Li, Z., Gao, J., Xing, X., Wu, S., Shuang, S., Dong, C., Paau, M.C. and Choi, M.M.F., **2010**. Synthesis and characterization of *n*-alkylamine-stabilized palladium nanoparticles for electrochemical oxidation of methane. *The Journal of Physical Chemistry C*, *114*(2), pp.723–733.
17. Yang, D.Q., Sun, S., Dodelet, J.P. and Sacher, E., **2008**. A facile route for the self-organized high-density decoration of Pt nanoparticles on carbon nanotubes. *The Journal of Physical Chemistry C, 112*(31), pp.11717–11721.
18. Raut, R.W., Haroon, A.S.M., Malghe, Y.S., Nikam, B.T. and Kashid, S.B., **2013**. Rapid biosynthesis of platinum and palladium metal nanoparticles using root extract of asparagus racemosus linn. *Advanced Materials Letters, 4*(8), pp.650–654.
19. Chen, J., Wang, M., Liu, B., Fan, Z., Cui, K. and Kuang, Y., **2006**. Platinum catalysts prepared with functional carbon nanotube defects and its improved catalytic performance for methanol oxidation. *The Journal of Physical Chemistry B, 110*(24), pp.11775–11779.
20. Goberna-Ferrõn, S., Soriano-Lõpez, J., Galán-Mascarõs, J.R. and Nyman, M., **2015**. Solution speciation and stability of cobalt-polyoxometalate water oxidation catalysts by X-ray scattering. *European Journal of Inorganic Chemistry*, *2015*(17), pp.2833–2840.

21. Duan, J., Song, L. and Zhan, J., **2009**. One-pot synthesis of highly luminescent CdTe quantum dots by microwave irradiation reduction and their Hg2+-sensitive properties. *Nano Research*, *2*(1), pp.61–68.

22. Hamizi, N.A. and Johan, M.R., **2010**. Synthesis and size dependent optical studies in CdSe quantum dots via inverse micelle technique. *Materials Chemistry and Physics*, *124*(1), pp.395–398.

23. Van Tam, T., Trung, N.B., Kim, H.R., Chung, J.S. and Choi, W.M., **2014**. One-pot synthesis of N-doped graphene quantum dots as a fluorescent sensing platform for Fe^{3+} ions detection. *Sensors and Actuators B: Chemical, 202*, pp.568–573.

24. Singh, P., Das, D., Kumar, A. and Singh, A.K., **2012**. Palladiumd (II) complexes of N-{2-(aryltelluro)ethyl}morpholine/piperidine: Synthesis, structure, application in Heck coupling and unprecedented conversion into nano-sized PdTe. *INOCHE, 15*, pp.163–166.

25. Chen, X., Li, L., Lai , Y. Lai, Yan, J., Tang, Y. and Wang, X., **2015**. Microwave-assisted synthesis of glutathione-capped CdTe/CdSe near-infrared quantum dots for cell imaging. *International Journal of Molecular Sciences*, *16*(5), pp.11500–11508.

26. Mai, X. and Hoang, Q., **2016**. The large-scale synthesis of vinyl-functionalized silicon quantum dot and its application in miniemulsion polymerization. *Journal of Nanomaterials, 2016*, pp.1–7.

27. Khatei, J. and Koteswara Rao, K.S.R., **2011**. Hydrothermal synthesis of CdTe QDs: Their luminescence quenching in the presence of bio-molecules and observation of bistable memory effect in CdTe QD/PEDOT:PSS heterostructure. *Materials Chemistry and Physysics*, *130*(1–2), pp.159–164.

28. Hou, B., Cho, Y., Kim, B.S., Hong, J., Park, J.B., Ahn, S.J., Sohn, J.I., Cha, S. and Kim, J.M., **2016**. Highly monodispersed PbS quantum dots for outstanding cascaded-junction solar cells. *ACS Energy Letters*, *1*(4), pp.834–839.

29. Liu, B., Ren, T., Zhang, J.R., Chen H.Y., Zhu, J.J. and Burda, C., **2007**. Spectroelectrochemistry of hollow spherical CdSe quantum dot assemblies in water. *Electrochemistry Communications*, *9*(4), pp.551–557.

30. Wu, W., He, Q. and Jiang, C.,**2008**. Magnetic iron oxide nanoparticles: Synthesis and surface functionalization strategies. *Nanoscale Research Letters*, *3*(11), pp.397–415.

31. Masikini, M., Ndangili, P.M., Ikpo, C.O., Feleni, U., Duoman, S., Sidwaba, U., Baker, P.G.L. and Iwuoha, E., **2016**. Optoelectronics of stochiometrically controlled palladium telluride quantum dots. *Journal of Nano Research, 40*, pp.29–45.

32. Bharara, M.S., Parkin, S. and Atwood, D.A., **2005**. Solution behavior of Hg(II)-cystamine by UV-Vis and Hg NMR. *Main Group Chemistry, 4*(3), pp.217–225.

33. Pietryga, J.M., Park, Y.S., Lim, J., Fidler, A.F., Bae, W.K., Brovelli, S. and Klimo, V.I., **2016**. Spectroscopic and device aspects of nanocrystal quantum dots. *Chemical Reviews, 116*(18), pp.10513–10622.

34. Shaik, M.R., Ali, Z.J.Q., Khan, M., Kuniyil, M., Assal, M.E., Alkhathlan, H.Z., Al-Warthan, A., Siddiqui, M.R.H., Khan, M. and Adil, S.F., **2017**. Green synthesis and characterization of palladium nanoparticles using origanum vulgare l. extract and their catalytic activity. *Molecules*, *22*(1), Article ID 165, 12 pages.

35. Kiplagat, A., Sibuyi, N.R.S., Onani, M.O., Meyer, M. and Madiehe, A.M., **2016**. The cytotoxicity studies of water-soluble InP/ZnSe quantum dots. *Journal of Nanoparticle Research, 18*(6), pp.1–12.

36. Cooper, J.K., Franco, A.M., Gul, S., Corrado, C. and Zhang, J.Z., **2011**. Characterization of primary amine capped CdSe, ZnSe, and ZnS quantum dots by FT-IR: Determination of surface bonding interaction and identification of selective desorption. *Langmuir*, *27*(13), pp.8486–8493.

37. Vo, N.T., Ngo, H.D., Phuong, N., Thi, D., Phung, K., THi, N., Duong, A.P. and Lam, V., **2016**. Stability investigation of ligand-exchanged CdSe/ZnS-Y (Y = 3-mercaptopropionic acid or mercaptosuccinic acid) through zeta potential measurements. *Journal of Nanomaterials, 2016*, pp.1-8.

38. Liang, G.-X., Gu, M.-M., Zhang, J.-R. and Zhu, J.-J., **2009**. Preparation and bioapplication of high-quality, water-soluble, biocompatible, and near-infrared-emitting CdSeTe alloyed quantum dots. *Nanotechnology*, *20*(41), Article ID 415103.

39. Rhieu, S.Y. and Reipa, V., **2015**. Tuning the size of gold nanoparticles with repetitive oxidation-reduction cycles. *American Journal of Nanomaterials*, *3*(1), pp.15–21.

40. Poznyak, S.K., Osipovich, N.P., Shavel, A., Talapin, D.V., Gao, M., Eychmüller, A. and Gaponik, N., **2005**. Size-dependent electrochemical behavior of thiol-capped CdTe nanocrystals in aqueous solution. *Journal of Physical Chemistry B, 109*(3), pp.1094–1100.

41. Grdeń, M., Łukaszewski, M., Jerkiewicz, G. and Czerwiński, A., **2008**. Electrochemical behaviour of palladium electrode: Oxidation, electrodissolution and ionic adsorption. *Electrochimica Acta*, *53*(26), pp.7583–7598.

42. Ghindilis, A.L., Atanasov, P. and Wilkins, E., **1997**. Enzyme-catalyzed direct electron transfer: Fundamentals and analytical applications. *Electroanalysis*, *9*(9), pp.661–674.

43. Yang, M., Kabulski, J.L., Wollenberg, L., Chen, X., Subramanian, M., Tracy, T.S., Lederman, D., Gannett, P.M. and Wu, N., **2009**. Electrocatalytic drug metabolism by CYP2C9 bonded to a self-assembled monolayer-modified electrode. *Drug Metabolism and Disposition*, *37*(4), pp.892–899.

44. Aliakbarinodehi, N., De Micheli, G. and Carrara, S., **2016**. Enzymatic and nonenzymatic electrochemical interaction of abiraterone (antiprostate cancer drug) with multiwalled carbon nanotube bioelectrodes. *Analytical Chemistry*, *88*(19), pp.9347–9350.

45. Dai, Z., Zhang, J., Dong, Q., Guo, N., Xu, S., Sun, B. and Bu, Y., **2007**. Adaption of Au nanoparticles and CdTe quantum dots in DNA detection. *Chinese Journal of Chemical Engineering*, *15*(029624), pp.791–794.

46. Feng, J.J., Zhao, G., Xu, J.J. and Chen, H.Y., **2005**. Direct electrochemistry and electrocatalysis of heme proteins immobilized on gold nanoparticles stabilized by chitosan. *Analytical Biochemistry*, *342*(2), pp.280–286.

47. Huang, H., Hu, N., Zeng, Y. and Zhou, G., **2002**. Electrochemistry and electrocatalysis with heme proteins in chitosan biopolymer films. *Analytical Biochemistry*, *308*(1), pp.141–151.

48. Iwuoha, E.I., Joseph, S., Zhang, Z., Smyth, M.R., Fuhr, U. and Ortiz De Montellano, P.R., **1998**. Drug metabolism biosensors: Electrochemical reactivities of cytochrome P450(cam) immobilised in synthetic vesicular systems. *Journal of Pharmaceutical and Biomedical Analysis*, *17*(6–7), pp.1101–1110.

49. Ross, N., Hendricks-Leukes, N., Ajayi, R.F., Baker, P. and Iwuoha, E. I., **2015**. Conductive composite biosensor system for electrochemical indinavir drug detection. *Journal of Chemistry*, *2015*, Article ID 630408, 7 pages.

50. Baj-Rossi, C., de Micheli, G. and Carrara, S., **2012**. Electrochemical detection of anti-breast-cancer agents in human serum by cytochrome P450-coated carbon nanotubes. *Sensors (Switzerland)*, *12*(5), pp.6520–6537.

51. Conner, K.P., Schimpf, A.M., Cruce, A.A., McLean, K.J., Munro, A.W., Frank, D.J., Krzyaniak, M.D., Ortiz De Montellano, P., Bowman, M.K. and Atkins, W.M., **2014**. Strength of axial water ligation in substrate-free cytochrome P450s is isoform dependent. *Biochemistry*, *53*(9), pp.1428–1434.

52. Belcher, J., McLean, K.J., Matthews, S., Woodward, L.S., Fisher, K., Rigby, S.E.J., Nelson, D.R., Potts, D., Baynham, M.T., Parker, D.A., Leys, D. and Munro, A.W., **2014**. Structure and biochemical properties of the alkene producing cytochrome p450 OleTJE (CYP152l1) from the jeotgalicoccus sp. 8456 bacterium. *Journal of Biological Chemistry*, *289*(10), pp.6535–6550.

Received: 4 October 2018. Accepted: 10 January 2019.